# Lamins regulate cell trafficking and lineage maturation of adult human hematopoietic cells

Jae-Won Shin[a], Kyle R. Spinler[a], Joe Swift[a], Joel A. Chasis[b], Narla Mohandas[b], and Dennis E. Discher[a,1]

[a]Molecular and Cell Biophysics Laboratory, University of Pennsylvania, Philadelphia, PA 19104; and [b]New York Blood Center, New York, NY 10065

Edited by Vann Bennett, Duke University Medical Center, Durham, NC, and approved October 1, 2013 (received for review March 15, 2013)

**Hematopoietic stem and progenitor cells, as well as nucleated erythroblasts and megakaryocytes, reside preferentially in adult marrow microenvironments whereas other blood cells readily cross the endothelial barrier into the circulation. Because the nucleus is the largest organelle in blood cells, we hypothesized that (*i*) cell sorting across microporous barriers is regulated by nuclear deformability as controlled by lamin-A and -B, and (*ii*) lamin levels directly modulate hematopoietic programs. Mass spectrometry-calibrated intracellular flow cytometry indeed reveals a lamin expression map that partitions human blood lineages between marrow and circulating compartments ($P = 0.00006$). B-type lamins are highly variable and predominate only in $CD34^+$ cells, but migration through micropores and nuclear flexibility in micropipette aspiration both appear limited by lamin-A:B stoichiometry across hematopoietic lineages. Differentiation is also modulated by overexpression or knockdown of lamins as well as retinoic acid addition, which regulates lamin-A transcription. In particular, erythroid differentiation is promoted by high lamin-A and low lamin-B1 expression whereas megakaryocytes of high ploidy are inhibited by lamin suppression. Lamins thus contribute to both trafficking and differentiation.**

rheology | biophysics | hematopoiesis | nucleus | mechanobiology

Hematopoietic cells that enter the circulation are seen to squeeze through small pores in the basement membrane and endothelium that partition bone marrow and blood (1). Retention within the marrow niche as well as trafficking into the circulation might therefore be regulated by cell deformability and the structural molecules responsible for it. Indeed, human polymorphonuclear neutrophils (PMNs) were shown decades ago to become more deformable upon differentiation in the marrow (2), with mature PMNs more capable of entering and exiting small capillaries (3). Leukemic cells are more rigid than normal, potentially explaining the interrupted blood flow and marrow hypercellularity in disease (4). Normal hematopoiesis has a well-characterized hierarchy, but it is unclear whether deformability factors into the program (3). Importantly, because of the high nucleus-to-cytoplasm ratio of hematopoietic cells, key processes such as sorting between marrow and blood could be based in part on nuclear deformability (Fig. 1*A*).

Lamins are intermediate filament proteins that assemble into "lamina" networks at the interface between chromatin and the inner nuclear membrane (5), conferring stiffness to the nucleus (6). In addition, the lamina is often proximal to heterochromatin, and, at least with embryonic stem cells, some genes alter their interactions with the lamina during cell-fate determination (7). In nearly all mammalian cells, A-type lamins (splice-forms A and C from *LMNA*) and B-type lamins (from *LMNB1* and *LMNB2*) are detectable. In blood progenitors versus various mature cells, past studies appear at odds, even for the same cell type in reporting either decreased levels of both lamins (8–10) or else increased levels (11). One dramatic mutation in human *LMNA* leads to the accelerated aging syndrome Progeria (5), in which protein accumulates at the nuclear envelope and stiffens it (12), affecting many tissues and increasing platelet numbers by two-fold or more (13). Mice with a large deletion in *LMNA* survive 6 wk postnatal (14), with defective lymphocytes (15), whereas mice deficient in the lamina-associated polypeptide 2α show hyperproliferation of erythroid progenitors and impaired differentiation (16). Relatively few mutations in B-type lamins have been reported (5), but defective lamin-B receptor in Pelger–Huet anomaly is characterized by hyposegmentation of neutrophils (17), defective chemotaxis, abnormal granulocytic differentiation, and also elevated lamin-A (18). Direct roles for lamins in normal human hematopoiesis, trafficking, and rheology otherwise remain unclear.

The synthesis and degradation of lamins is understudied in hematopoiesis. However, it is known that the lamin-A promoter has a retinoic acid (RA)-responsive element (19), and RA therapy for acute promyelocytic leukemia stimulates granulocyte differentiation (20) and decreases lamin-A expression, consistent with the early report of increased deformability of normal mature PMN (2). T cells also up-regulate lamin-A upon stimulation with phytohemagglutinin (21) although a functional effect is unknown. B-type lamins undergo proteolytic cleavage during early erythroid differentiation from burst forming unit-erythroid (BFU-E) and colony forming unit-erythroid (CFU-E) to pro-erythroblast (ProEry) stage via caspase-3 activation (22), and, in later stages, a distinct decrease in B-type lamins parallels the decrease in nuclear volume (23). The generality of such processes and their impact on nuclear flexibility are examined here.

High nuclear flexibility or compliance, with suitably low lamin levels, might facilitate migration of nucleated cells through constraining pores. On the other hand, the Erythroid (Ery) lineage undergoes nuclear condensation, which might stiffen the nucleus and limit trafficking but permit enucleated reticulocytes to egress more readily through small pores. Megakaryocytes (MK) undergo polyploidization, and the mature nucleus could be too large to pass through pores: such "nuclear anchorage"

## Significance

**Comparing human blood cell types, nuclear diversity is visually striking but unexplained: quasi-spherical nuclei in stem/progenitor cells and T cells contrast with multilobed nuclei in neutrophils, giant nuclei in megakaryocytes, and anuclear erythrocytes. We hypothesized broad roles for the major nuclear structure proteins—lamins—and developed mass spectrometry-calibrated intracellular flow cytometry to quantify lamin-A:B ratios. This ratio controls both nuclear viscoelasticity and cell trafficking across microporous barriers. High A:B rigidifies erythroblast nuclei to favor marrow retention and also enhances erythropoiesis. Intermediate A:B enhances thrombopoiesis and opposes cell division to favor marrow anchorage of megakaryocytes. Human stem/progenitor cells have moderate lamin levels and reside in marrow whereas white cells are favored by low lamins and predominantly circulate.**

Author contributions: J.-W.S., J.S., J.A.C., N.M., and D.E.D. designed research; J.-W.S., K.R.S., and J.S. performed research; N.M. contributed new reagents/analytic tools; J.-W.S., K.R.S., J.S., J.A.C., N.M., and D.E.D. analyzed data; and J.-W.S., J.S., J.A.C., N.M., and D.E.D. wrote the paper.

The authors declare no conflict of interest.

This article is a PNAS Direct Submission.

[1]To whom correspondence should be addressed. E-mail: discher@seas.upenn.edu.

This article contains supporting information online at www.pnas.org/lookup/suppl/doi:10.1073/pnas.1304996110/-/DCSupplemental.

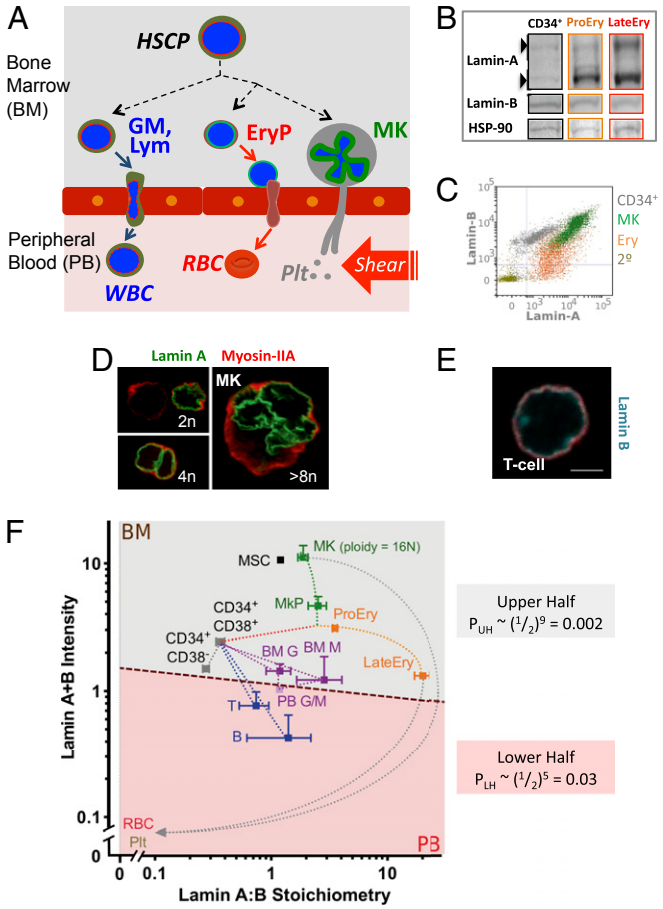


**Fig. 1.** Lamin map of human hematopoiesis. (*A*) Hematopoietic cells are mostly in marrow or blood, and only a fraction of cells transmigrate through the endothelium with or without their nucleus. EryP, erythroid progenitors; GM, granulocytes and monocytes; HSCP, hematopoietic stem cell and progenitors; Lym, lymphocytes; MK, megakaryocytes; RBC, red blood cells; WBC, white blood cells. (*B*) Validation of flow cytometry by Western blot with cell numbers adjusted to give similar intensities of B-type lamins. Lamin-A,C splice-forms and B-type lamins are shown for fresh $CD34^+$, early and late erythroid cells; densitometry shows rough agreement with MS-IF results. (*C*) Representative intracellular flow cytometry scatterplots show lamin-A (Alexa-488) and B-type lamin (Alexa-647) expression for indicated cells. (*D*) Confocal images of MKs immunostained for lamin-A (green) and myosin-II (red). (*E*) Confocal image of T cell immunostained for B-type lamins (cyan) and myosin-II (red) (Scale bar: 5 μm.) (*F*) Lamin-A relative to B-type lamins, transformed to a measurable A:B ratio versus calibrated sum intensity A+B (a.u.); on log scales, these are the respective difference and sum of chemical potentials for A and B (Fig. S2*A*). Mean fluorescent intensity of lamin for each subpopulation from flow cytometry was calibrated to an absolute ratio from MS analyses of a standard A549 cell line (lamin-A:B = 2.3) (Fig. S1). The dashed line schematically illustrates the semipermeable barrier between bone marrow (BM) and peripheral blood (PB), and the net probability of partitioning based on lamin expression can be estimated from the upper half and lower half probabilities: $P_{TOT} = P_{UH}\,P_{LH} = 0.00006$. Measurements are mean ± SEM of $n \geq 3$, with error bars omitted if <5% of mean. BM G, BM granulocytes ($CD33^{mid}$); BM M, BM monocytes ($CD33^{hi}$); $CD34^+CD38^-$, early progenitors; $CD34^+CD38^+$, common progenitors; LateEry, late erythroblasts ($CD44^-GPA^+$); MK, polyploid MKs (average 16N); MKP, MK progenitors ($CD34^-CD41^+$); MSC, mesenchymal stromal cells; PB G/M, PB granulocytes/monocytes; Plt, platelets; ProEry, proerythroblasts ($CD44^+GPA^-$); RBC, red blood cells; T, B, lymphoids. Representative MSC results from one donor are shown because the variation in A:B ratios between donors and cultured cells was minimal.

would permit MKs to extend motile membrane projections into blood so that shear fragmentation could produce platelets—as visualized recently (24). To investigate functional roles of lamins in differentiation-modulated trafficking, we began by determining the levels and stoichiometry of lamins in major lineages, uncovering a systematic expression map.

## Results

**Lamin-Based Lineage Map Sorts Marrow and Peripheral Blood.** Expression of both lamin-A and B-type lamins throughout hematopoiesis was assessed with antibodies in Western blotting, flow cytometry, and confocal microscopy (Fig. 1 *B–E*). To quantify lamin isoforms in terms of absolute stoichiometry within a given hematopoietic cell type (including rare cells), we applied a single-cell method of mass spectrometry-calibrated intracellular flow cytometry (MS-IF) (Fig. S1). In the flow cytometer, antibodies against surface markers first identify a cell type in a mixed population of cells whereas intracellular immunostaining for lamins provides relative intensity measures of lamins. Relative intensities are then calibrated by similar measurements on a standard cell line with lamin stoichiometry that has been quantified by mass spectrometry (*Materials and Methods*). Unlike solid tissues where B-type lamins are often "constitutive" (5), B-type lamins vary here by ~30-fold in diploid cells whereas lamin-A varies much less (Table S1). MS-IF reveals the lowest lamin-A:B ratio ~ 1:4 in $CD34^+$ cells (mostly progenitors) whereas Erythroblasts (Ery) exhibit the highest A:B ratio [~100-fold higher for LateEry: glycophorin A $(GPA)^+$, $CD44^{lo/-}$]. At the same time, the total intensity (A+B) is nearly constant as summarized in a "map" of sum-versus-ratio for lamins in hematopoietic cells (Fig. 1*F*). A modest two- to threefold decrease in A+B from ProEry (ploidy of 2n, and some premitotic 4n) to LateEry (2n) is consistent with loss of B-type lamins and a smaller nuclear area (23). Although this observation reveals an isoform switch from B to A before Ery enucleation, it establishes together with the low A:B ratio in CD34+ cells a very broad A:B range.

MK lineages show an intermediate A:B ratio, but, during maturation, they up-regulate both types (A+B) by up to 10-fold (Fig. 1*F* and Table S1). Even for MK progenitors (MKP) of low ploidy (2n, 4n cells), lamins increase about fivefold relative to $CD34^+CD38^-$. Further A+B increases in late MK (~16n) are likely due to lamins accumulating in high ploidy nuclei because lamins interact with chromatin (Fig. 1*D*) (7). The extremes in lamin expression (A:B for Ery, and A+B for MK) seem consistent with the hypothesis, as examined by biophysical methods below, that nuclear rigidity and/or size limit nuclear entry into small pores and marrow sinusoids. As a consequence, human RBCs are enucleated, and the resultant lamin-less reticulocytes traverse the endothelium. Motile membrane projections likewise extend from MKs into blood, allowing platelets to be generated by blood-shear fragmentation.

Nucleated lineages that traffic into blood have lower lamin levels than Ery and MK. Lymphoid cells in blood show only ~sixfold higher A:B ratio compared with CD34+ cells but nearly 10-fold lower A+B, with similar trends for granulocyte/monocyte (G/M) lineages (Fig. 1 *E* and *F* and Table S1). On the other hand, marrow-resident mesenchymal stromal cells (MSCs) are not found in circulation, and their total lamin levels are similar to late MK despite the low ploidy of MSCs.

In the lineage map of lamins (Fig. 1*F*), a simple line is drawn that separates all marrow-resident cells from all peripheral blood cells. The upper half of this map has the nine measured cell types that are predominantly in marrow, and the lower half has the five cell types that are predominantly in circulation (Tables S2–S4). The probability of such a simple partitioning with all $lamin^{hi}$ in the marrow "Upper Half" (UH: $P_{UH} = 0.002$) and all $lamin^{lo}$ in the blood "Lower Half" (LH: $P_{LH} = 0.03$) is estimated to be $P_{TOT} = 0.00006$. The endothelium is, after all, a barrier that physically partitions two cellularized compartments, and what sets the probability of crossing that barrier is the ability of a given cell to move and deform through the small pores of the boundary (Fig. S2).

**Lamin-A Limits 3D Migration of Nucleated Hematopoietic Cells.** Transendothelial migration involves large deformation as nucleated cells pass through much smaller pores (3), and we hypothesized that transwell filters with different size micropores could be used to show that lamin-A knockdown will enhance constrained migration (Fig. 2*A*). Aspiration of a cell into a micropipette illustrates the requisite nuclear deformation (e.g., G/M cells, Fig. 2*B*). Our previous aspiration experiments on a lung epithelial cell line showed that disruption of the cytoskeleton with or without lamin knockdown can reveal the contribution of lamins to nuclear properties (6). This previous study prompted a similar approach here, but with care to use low stresses commensurate with those generated by cells during migration (25). With G/M cells, lamin-A knockdown by ~50% (Fig. S3*A*) indeed softens the nucleus ~twofold (Fig. 2*B*). We hypothesized therefore that lamins in intact cells should also regulate migration through transwell filters. Using a broad range of filters, we tested whether migration would be impeded when cells squeeze through micropores similar to the size of blood capillaries (~3 μm) whereas migration through large pores would be unaffected.

Migration of different hematopoietic lineages across the different filters was driven (in 4 h) by a standard chemotactic gradient of stromal derived factor-1 (SDF-1). For 3-μm pores, the percentage of cells that migrated is lowest for both $CD34^+$ cells and MKs, but, for 8-μm pores, the majority of $CD34^+$ cells cross the filter whereas the percentage of migrated MKs was relatively unchanged. Such transwell results seem qualitatively consistent with finite numbers of circulating $CD34^+$ cells compared with no measurable MKs (Tables S2–S4). Given that the percentage of migration within a set assay time relates to migration velocity and also because pore area relates inversely to the requisite stress for migration through the constriction, the migration data are fit to a standard hyperbolic "Hill" equation for "velocity versus force" motility. The pore area for half-maximal migration of each lineage ($A_{1/2}$) could thus be estimated. Although the general trend is that $CD34^+$ and T-cells have a low $A_{1/2}$, and the "extreme" cell types in the lineage map, such as high ploidy MKs, have a high $A_{1/2}$ (Fig. 2*C* and Fig. S3*B*), this parameter correlates weakly with lamin A+B or A:B stoichiometry (Fig. S3*C*). Instead, the change in percent migration with change in pore size (*Materials and Methods*) reveals the migration sensitivity to pores, and the lineage-dependent migration sensitivity for small pores (3 μm) correlates well with lamin-A:B stoichiometry (Fig. 2*D*) (and not A+B, Fig. S3*D*). In other words, cells with lower A:B are less sensitive to pore size; conversely, cells with higher A:B are more sensitive to pore-size differences.

To determine whether lamin-A directly influences cell migration through a constraining micropore, siRNA knockdown was used. The percentage of $CD34^+$-derived granulocyte/macrophage cells migrating through 3-μm or 5-μm pores increased by about twofold after knockdown (Fig. 2*E*), which approximates the measured softening in Fig. 2*A*. Importantly, no significant change was observed with 8-μm pores, which indicates that lamin-A limits migration of cells only through small pores. Knockdown of lamin-A did not change the expression levels of other proteins typically involved in migration through pores, such as myosin-II (26). These results indicate a major role for lamin-A in regulating pore trafficking.

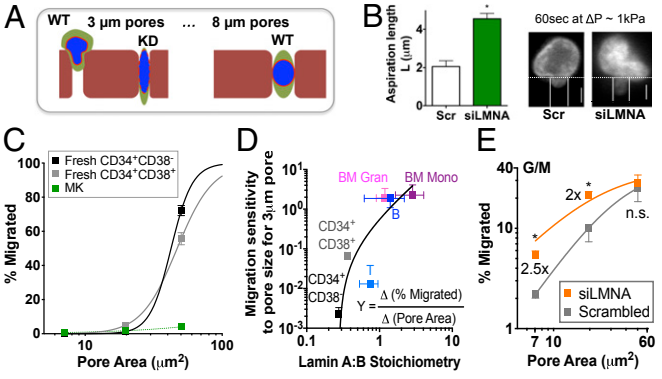


**Fig. 2.** Lamin-A:B regulates transmigration of nucleated blood cells. (*A*) Schematic illustration of hypothesis that cell migration and nuclear deformation through sufficiently small micropores will be facilitated by lamin knockdown (KD). (*B*) Lamin-A confers nuclear stiffness, based on aspiration of G/M cells with or without knockdown with lamin-A siRNA (siLMNA). (*Left*) Quantitation of aspirated nuclear length ($n = 3$ donors, $^*P < 0.05$). (*Right*) Representative image is for $\Delta P < 1$ kPa at 60 s. (Scale bars: 5 μm.) (*C*) Migration of fresh $CD34^+$ and MK cells. Cells were incubated on top of transwell with different pore sizes (3, 5, or 8 μm) with an SDF-1 (100 ng/mL) gradient for 4 h before analysis by flow cytometry to evaluate % migrated cells. Data were fit to $y = a/[1 + b(x\text{-}x_c)^{-m}]$, where y = %migrated, x = pore area ($\mu m^2$), a = 100 (% maximal migration when pore size is infinite), b relates to the half-maximum migration area (Fig. S3*C*), $x_c$ = critical pore area, m = Hill coefficient. Values for b, $x_c$, and m for each cell type are as follows: $CD34^+CD38^-$ (0.024, 1.44, and 5.4, respectively), $CD34^+CD38^+$ (0.022, 1.44, and 3.2, respectively), MK (0.0006, 0, and 0.9, respectively). (*D*) Lamin ratios predict migration sensitivity to pore size at small pores: the first derivative of y(x) was estimated for 3-μm pores and then fit to a power law yielding $Y(\text{at } 3\ \mu m) = 0.90\ (\text{A:B} - 0.28)^{1.55}$ ($R^2 > 0.95$). (*E*) Lamin-A limits 3D migration. Before transwell migration, cells were transfected with siLMNA for 3 d to give ~50% knockdown (Fig. S3*A*). Results from granulocyte/macrophage cells derived from $CD34^+$ culture are shown. Data fit per *C*. All results are mean ± SEM of $n \geq 3$. $^*P < 0.05$ in paired *t* test.

**Lamin Isoform Stoichiometry Predicts Nuclear Rheology.** Of the many studies of hematopoietic cell deformability (e.g., ref. 2), nuclear deformability has not yet been directly characterized and compared across lineages. We had shown that fresh human $CD34^+$ cells are highly deformable compared with solid-tissue cell types (6), perhaps indicative of the stem cell/progenitor's ability to traffic between marrow and circulation. The progressive increase in aspirated length of a nucleus at a constant pressure (Fig. 3*A*) gives the nuclear compliance and often fits a power law $J(t) = a \cdot t^b$ that is typical for polymer rheology (6). The initial compliance is given by *a*, whereas $b = 1$ indicates a simple fluid that flows and does not recover after release of stress, and $b = 0$ indicates a simple elastic solid that will fully recover its shape.

Lymphoid and myeloid nuclei show high initial compliance ($a = 20\ kPa^{-1}$) (Fig. 3*A*), as predicted from their low lamin levels (Fig. 1*B*), and are roughly similar in this respect to fresh $CD34^+$ cells (6). T-cell nuclei are also more viscous ($b = 0.22$) than myeloid nuclei ($b = 0.08$) (Fig. 3*A*), consistent with a previous report that granulocytes do not permanently deform as they pass through marrow (3). In contrast, Ery progenitors generally show at least 10-fold lower initial nuclear compliance (Fig. 3*A*). Although ProEry nuclei exhibit viscoelastic behavior similar to that of T-cell nuclei, late Ery nuclei are completely stiff and solid, consistent with their condensation during terminal differentiation. MK nuclei also have lower initial compliance than myeloid or lymphoid nuclei. Compared with MK progenitor nuclei (with $b = 0.47$), mature MK nuclei have 20-fold higher compliance despite being more solid-like ($b = 0.11$) (Fig. 3*A*). The large size and complex shape of polyploid MK nuclei, rather than compliance itself, are therefore likely to limit MK traffickability. Consistent with this, lamin-A:B stoichiometry correlates strongly with local nuclear stiffness [reciprocal of compliance 1/J(t) in Fig. 3*B*] measured at different time points (Fig. S4*A*), which is not the case for A+B intensity (Fig. S4*B*).

Given that B-type lamins localize to the lamina during erythroid differentiation (23) and that nuclear stiffness increases with lamin A:B (Fig. 3*B*), we hypothesized that down-regulation of B-type lamin(s) would effectively stiffen the nucleus during maturation. Typically, one expects that stiffness correlates positively with protein abundance, and so the prediction here is highly unusual for biopolymer physics. ProEry indeed shows decreased expression of B-type lamins compared with fresh $CD34^+$ cells (Fig. 1*F* and Table S1), and nuclear stiffness of ProEry is high

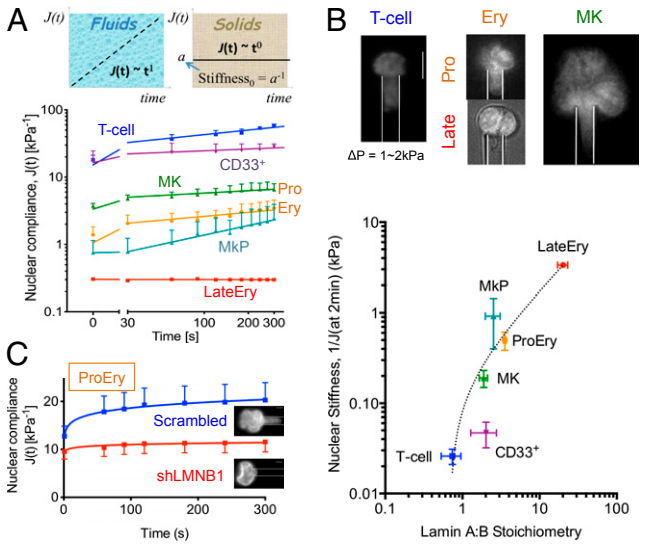


**Fig. 3.** Lamin ratios predict nuclear stiffness in hematopoietic lineages. (*A*) Nuclear compliance change versus time at constant pressure $\Delta P = 0.3$–6 kPa. (*Upper*) A power law fit, $J(t)$ ($kPa^{-1}$) = $a \cdot t^b$ (t = sec) for each blood cell type, where (b = 1 for fluids), (b = 0 for solids). (*Lower*) Values for (a, b) in each cell type are as follows: (T cell: 15.2, 0.2), ($CD33^+$: 16.4, 0.1), (MkP ≥ 30s: 0.16, 0.5), (MK: 3.4, 0.1), (ProEry: 1.1, 0.2), (LateEry: 0.3, 0). (*B*) High lamin-A:B correlates with stiff nuclei. (*Upper*) Images at 2 min of nuclear aspiration at $\Delta P = 1$–2 kPa. (Scale bar: 5 μm.) (*Lower*) Correlation between nuclear stiffness (at 2 min) and lamin-A:B fits J (at 2 min) = $0.23(\text{A:B} - 0.68)^{0.91}$ ($R^2 = 0.96$). All results are mean ± SEM of $n \geq 5$ for each cell type. (*C*) Lamin-B1 knockdown stiffens nuclei in proerythroblasts, with no change in viable cell numbers ($n = 10$, $P < 0.05$). Nuclear compliance change with $\Delta P = 1$–2 kPa where values for (a, b) in each sample are as follows: (scrambled: 12.8, 0.1), (shLMNB1: 9.4, 0.03). (Scale bars: 5 μm.)

compared with circulating nucleated cells (Fig. 3*A*). To directly address the hypothesis, we knocked down lamin-B1, which is expressed at much higher levels than lamin-B2 in hematopoietic cells based on mass spectrometry analyses (Tables S5 and S6). In erythroid precursors, partial knockdown of lamin-B1 by RNAi (~50%) (Fig. S4*C*) increases nuclear stiffness (Fig. 3*C* plot shows decreased compliance). Nuclear stiffening after lamin-B1 knockdown was also measured for a U251 glioma cell line in which the lamin-B1 isoform is only slightly more abundant and where knockdown-induced differentiation is unlikely (Fig. S4*D*). Lamin-B1 down-regulation in erythroid lineages is thus sufficient to promote nuclear stiffening, which is likely to favor marrow retention of a cell (Fig. 1). A preliminary study using pharmacological perturbations of erythropoietic pathways suggests the association with nuclear rigidification (Fig. S5).

**Lamins Modulate Differentiation: Erythroid Lineage.** Recent studies of a few primary cells have shown significant modulation of differentiation by lamins. In particular, lamin-A overexpression in marrow-derived MSCs increases osteogenesis (27) whereas knockdown promotes adipogenesis (28). However, lamin knockout mice develop all tissue types before succumbing at birth or shortly after (14, 29), and so most or all tissue lineages seem to develop to some extent, which implies lamins function as lineage maturation factors. Here, we manipulated lamin levels in those hematopoietic lineages with extreme expression, Ery and MK, to assess direct modulation of differentiation (Fig. 4*A*).

Overexpression of lamin-A by ~threefold in $CD34^+$ cells (Fig. S6*A*) is close to the increased level measured during erythropoiesis (Fig. 1*F*) and resulted in a significant shift toward BFU-E from colony forming unit (CFU)-granulocyte and macrophage (GM) (Fig. 4*B*), consistent with the map (Fig. 1*F*). The multipotent CFU-granulocyte erythroid macrophage megakaryocyte (GEMM) was unaffected (Fig. 4*B*). B-type lamins decrease during erythroid development (22, 23) (Fig. 1*F*), and knockdown of lamin-B1 by RNAi in early hematopoietic progenitors indeed favors BFU-E (Fig. 4*C*). In addition, lamin-B1 RNAi decreases CFU-GEMM in contrast to lamin-A overexpression, revealing lamin-B1 as more influential to the maintenance of multipotent progenitors. The results thus show that lamins regulate lineage specification induced by soluble factors.

**Lamins Modulate Differentiation: MK Lineage.** MKs normally show an increase in total lamin levels (Fig. 1*F*), but also an increase in A:B ratio. Overexpression of lamin-A indeed increases the number of both early and late MK progenitors cultured from BM $CD34^+$ cells based on surface markers (Fig. 4*D*). Furthermore, although lamin-B1 knockdown suppresses polyploid and 4n populations (Fig. 4*E*), overexpression of lamin-A enhances polyploidy (Fig. S6*B*). Because Progeria patients reportedly have twofold more platelets in circulation (13), we also tested the impact of the progerin mutant (Δ50) on MK polyploidy. Overexpression of progerin, which tends to drive lamin accumulation at the envelope (12), does not greatly enhance the number of 8n MKs, but both wild-type and mutant overexpression increase high ploidy (≥16n) MKs (Fig. S6*B*). The finding here that overexpression of both wild-type and progerin lamin-A gave the same phenotype is consistent with similar findings of increased osteogenesis in MSCs (27), suggesting a common mechanism of increased lamina assembly.

Phosphorylation of lamin-A promotes disassembly and is high during cell division (30), and so we hypothesized that an S22A

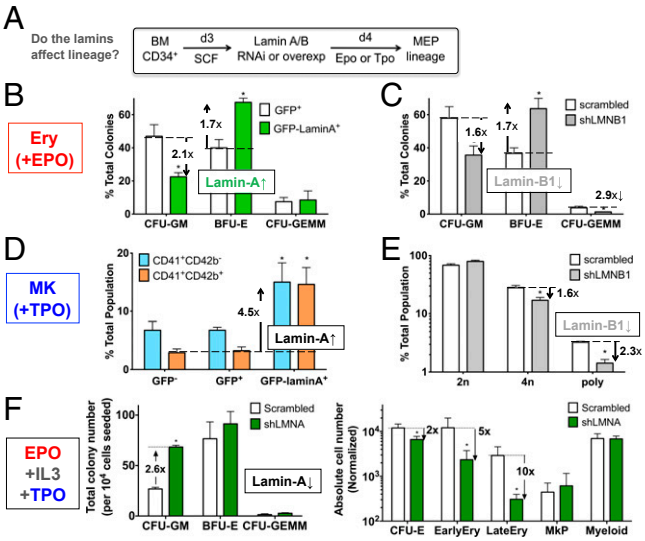


**Fig. 4.** Lamins regulate erythroid and MK differentiation. (*A*) Scheme for in vitro differentiation. MEP, myeloid and erythroid progenitor; SCF, stem cell factor. Epo is erythropoietin and induces erythropoiesis; Tpo is thrombopoietin and induces MK-poiesis. (*B* and *C*) Colony-forming assays in methylcellulose medium show a shift to erythroid progenitors after (*B*) overexpression of GFP-lamin-A (~40% transfection efficiency) or (*C*) knockdown of lamin-B1 (shLMNB1, ~50% efficiency) in the presence of Epo for 3 d. $^*P < 0.05$, GFP vs. GFP-lamin-A or scrambled vs. shLMNB1 ($n = 3$). (*D* and *E*) MK progenitor population enumerated by flow cytometry with CD41 and CD42b. (*D*) MK progenitors increase with lamin-A overexpression. $CD41^+CD42b^-$, early progenitor; $CD41^+CD42b^+$, late progenitor. $^*P < 0.05$, $GFP^+$ vs. GFP-lamin-$A^+$ for each progenitor ($n = 4$). (*E*) Lamin-B1 knockdown decreases average MK ploidy. $^*P < 0.01$, scrambled vs. shLMNB1 ($n = 3$). (*F*) Lamin-A is required for erythroid differentiation and restricts myeloid progenitor number. Cells were transduced with either scrambled or lamin-A shRNA (shLMNA) and cultured in the presence of Epo, IL-3 and Tpo. Functional progenitors (CFU-GM, BFU-E, CFU-GEMM) were quantified by colony-forming assay (*Left*) whereas differentiated subpopulations were quantified by flow cytometry as per ref. 39 (*Right*), normalized by $10^4$ initial cell number. CFU-E, $CD34^-CD36^+IL\text{-}3R^-$; EarlyEry, $CD44^+GPA^+$; LateEry, $CD44^-GPA^+$; MkP, $CD41^+$; Myeloid, $CD33^+$. $^*P < 0.05$, scrambled vs. shLMNA.

mutant that cannot be phosphorylated would limit nuclear division and again facilitate polyploidization. Overexpression of this mutant indeed shows a greater gain in 8n MKs than WT (Fig. S6*B*). Overall, the MK results suggest that, whereas lamina regulatory mechanisms might play a role during the formation of early polyploid MKs, the accumulation of lamin-A content per se appears sufficient to drive the formation of late polyploidy MKs through unknown mechanisms.

**Lamin-A Modulates Lineage Decisions.** Lamin-A knockdown with shRNA (~75% efficiency) (Fig. S6*C*) was performed to assess fate choices in the presence of a cytokine mixture that promotes multiple lineages (myeloid, erythroid, and MK). In such cultures, knockdown increases the total number of CFU-GM (Fig. 4*F*, *Left*) but decreases CFU-E and differentiated erythroid lineages without affecting BFU-E or the other differentiated lineages (Fig. 4*F*, *Right*). Together with the restriction of BFU-E by lamin-B1 (Fig. 4*C*), the results confirm predictions from the lamin map (Fig. 1*F*) that lamin-A and B1 play opposite roles in erythroid differentiation.

**Lamin-A Is Modulated by Physiological Agonists in Differentiation.** Retinoic acid (RA) in human serum normally is about 12 nM, and the lamin-A promoter is known to have multiple RA-responsive elements (19). RA is also known to promote terminal differentiation of granulocytes and self-renewal of hematopoietic stem cells while decreasing erythroid progenitor numbers (30, 31). Indeed, the RA receptor antagonist AGN194310 (AGN) increases granulocyte progenitors in mice by twofold, by blocking differentiation, with no significant effect on other lineages (31). Here, sustained RA treatment not only enhances both the number and size of myeloid colonies under G-CSF (Fig. 5*A* and Fig. S6 *D* and *E*), but also enhances migration of $CD34^+$ progenitors through 3- to 5-μm pores (Fig. 5*B*). The ~twofold effect is similar to the gain seen with direct lamin-A knockdown (Fig. 2*E*) and once again shows no significant impact on migration through the largest, nonconstraining pores (8 μm) (Fig. 5*B*). Indeed, RA represses lamin-A but not B-type lamin protein expression by ~twofold for both $CD34^+$ and $CD34^-$ cells (Fig. 5*C*). As predicted from the previous promoter analysis (19), the repression (~twofold) occurs at the transcriptional level as indicated by lamin-A promoter activity measured here (Fig. 5*D*). The results are consistent with the role of lamin-A in suppressing the myeloid progenitor number (Fig. 4*F*, *Left*).

The effects of RA on lamin-A levels seem to also apply to erythroid lineages, repressing lamin-A when $CD34^+$ cells are treated with Epo supplemented medium (Fig. 5*E*, *Inset*). Consistent with the lamin map (Fig. 1*F*), RA suppresses erythroid colony formation in a dose-dependent manner (Fig. 5*E*): the ~12 nM RA in human plasma is insufficient to suppress erythroid number, but a therapeutic dose for acute promyelocytic leukemia (~1 μM peak in plasma) (20) inhibits erythroid differentiation ~30-fold. AGN rescues both erythroid colony number and lamin A:B ratios in the presence of RA, but AGN has no effect on its own (Fig. 5*E*). Because pharmacological actions on nuclear receptors involve cell type-specific cofactors (32), AGN as a neutral antagonist in erythroid differentiation could reflect differences in cofactor expression. The results nonetheless indicate that RA regulates lamin-A, and the knockdown and overexpression studies indicate that lamin-A changes are sufficient to influence lineage.

## Discussion

The epigenetic changes of lineage specification are likely affected by the nuclear lamina, which might selectively, if indirectly, interact with different chromatin regions during differentiation (7). Here, we show roles of the lamins in deformability-based sorting as well as lineage induction of blood cells. This characterization of lamin expression stoichiometry in freshly isolated hematopoietic cells from human marrow and blood demonstrates that absolute lamin A:B ratios correlate with nuclear stiffness (Fig. 3*B*). Although prior studies suggest that lamin-A is "below the detection limit"

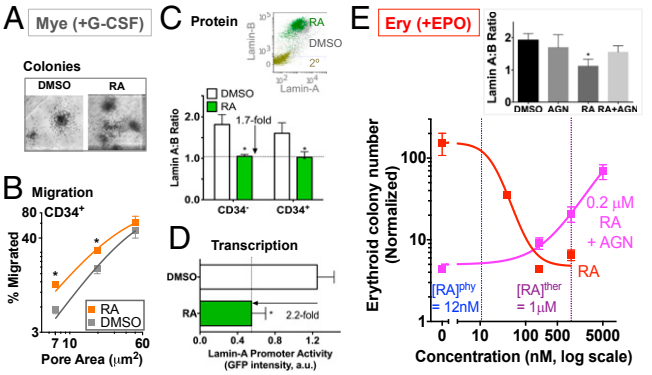


**Fig. 5.** Lamin-A levels change with physiological agonists. (*A*) Retinoic Acid (RA) modulates lamin-A in myeloid (Mye) differentiation. $CD34^+$-derived cells treated with either DMSO or RA (1 μM) for 3 d with G-CSF (10 ng/mL) before assays. CFU-GM colonies are more abundant and larger with RA (Fig. S6 *D* and *E*). (*B*) Effect of RA on transwell migration of $CD34^+$ cells. $*P < 0.05$ ($n = 3$) for DMSO vs. RA in paired *t* tests (unless noted). (*C*) RA down-regulates lamin-A protein expression for both $CD34^-$ and $CD34^+$ cells. (*Inset*) A representative flow cytometry plot (2°, secondary alone). $*P < 0.01$, DMSO vs. RA ($n = 4$). (*D*) RA represses lamin-A transcription. Cells were transiently transfected with a GFP reporter construct driven by a human lamin-A promoter, consisting of the 1,132-base pair upstream region and the first 385-base pair mRNA transcript region, followed by drug treatment. $*P < 0.05$ ($n = 4$). (*E*) RA modulates lamin-A in erythroid (Ery) differentiation. Absolute values of erythroid colony numbers were normalized to initial cell input and fit to dose–response curves. ($IC_{50}$ or $EC_{50}$, Hill coefficient) for: RA (20 nM), AGN in the presence of 0.2 μM RA (250 nM). $R^2 > 0.9$. ($n = 3$). (*Inset*) Lamin A:B ratios with drug treatment (AGN: 5 μM, RA: 0.2 μM). $*P < 0.05$, one-way ANOVA ($n = 3$). All results are mean ± SEM.

in terminally differentiated myeloid and lymphoid cells (8), another study suggested that it is restricted to the late stage of lymphoid development but not the early (11). Some studies suggest that B-type lamins are constitutive (9, 11) whereas other studies indicate that they are down-regulated in primary neutrophils (10). One study also acknowledges that, whereas blood granulocytes have much lower levels of both lamin-A and -B than the granulocytic HL-60 cell line, both lamins are detectable by confocal microscopy with distinct polymorphonuclear morphology (10). Our efforts to take a standardized approach with MS-IF show that A- and B-type lamins are generally present across different blood-cell types and at different levels. Although our data support some prior studies that total lamin expression is significantly decreased in both lymphoid and myeloid lineages upon differentiation from progenitors ($CD34^+CD38^+$), lamin A:B ratios are increased to ~1 (Fig. 1*F*) and correlate with the known distribution of these lineages in marrow versus blood (Tables S2–S4).

Because most small openings between endothelial cells in marrow sinusoids are filled by marrow cells in situ (3), nuclear stiffness seems a reasonable limiting factor. Although it was previously appreciated that granulocytes are highly traffickable due to their unique polymorphonuclear morphology, our study reveals that T cells may be even more amenable to trafficking than granulocytes due to (*i*) lower lamin A:B ratio (Fig. 1*F*), (*ii*) lower marrow:blood cell ratio (Tables S2–S4), (*iii*) lower nuclear stiffness (Fig. 3*B*), and (*iv*) lower half-maximal pore area for migration (Fig. S3*C*). In contrast, although MK nuclei remain deformable (Fig. 3*A*), their size and complex morphology generally limit MK migration through small pores. Intact MKs could therefore be occasionally observed in circulation, but further chromatin condensation after exhaustive platelet generation would tend to inhibit traffickability (3). Flow-cytometry analyses of what crosses the micropore filters in our MK experiments indeed show that many more small-cell fragments (e.g., platelet-like particles) traffic across than cells (Fig. S7), consistent with the platelet-generating scheme in Fig. 1*A*.

Although lamin-A,C splice-form ratios require further study, a major finding here is that lamin-B1 regulates lineage specification as well as nuclear stiffening. Consistent with wide variation in lamin A:B ratios between neuronal cell types (33) and between solid tissue cell types in general (34), our measurements of absolute stoichiometry demonstrate widely differing ratios of A- and B-type lamins in hematopoiesis, which might reflect selective cleavage of B-type lamins during early erythropoiesis (22) and general accumulation of lamins during MK polyploidization (35). One previous study of mouse embryonic fibroblasts suggested that lamin-B1 does not contribute to nuclear mechanics, but such cells could be dominated by lamin-A (36). In contrast, during late erythroid differentiation here, reduction of lamin-B1 by knockdown as well as inhibition of HSP90 or histone acetylation stiffens the nucleus. Because avian erythrocytes undergo chromatin condensation without enucleation and no large change in lamin-B1 was observed in late murine erythropoiesis (37), detailed mechanisms of nucleus-based sorting and lamin regulation could be species specific.

Our results indicate that lamin-A:B stoichiometry defines nuclear stiffness, indicating separable roles as distinct polymers in defining viscoelasticity of nuclei. Given that decreasing lamin-A softens nuclei (6) (Fig. 2*B*) and that migration sensitivity to pore size increases as the relative amount of lamin-A increases (Fig. 2*D*), lamin-A dictates time-dependent deformability, which is indicative of a viscous fluid. On the other hand, lamin-B1 confers nuclear elasticity and resilience (Fig. 3*C*) so that its decrease during erythropoiesis produces a nucleus that is slow to recover and effectively stiffer. These results are consistent with previous measurements by fluorescence correlation spectroscopy (38) showing lamin-A is more mobile than B-type lamins. Our studies already implicate RA as a physiological factor in lamin-A expression (Fig. 5), but additional soluble or insoluble factors could likewise influence lamin levels, lineage, and cell trafficking.

## Materials and Methods

Cell culture, micropipette analyses, pore migration assays, and other standard techniques are described in *SI Materials and Methods*. Commercially available primary human cells from marrow were obtained from either AllCells, Inc. (Emeryville, CA) or anonymous donors to the University of Pennsylvania Stem Cell Core with University of Pennsylvania Institutional Review Board approval ($n > 10$). Because lamins vary greatly across hematopoietic cells and because a standard method such as immunoblotting is a (nonlinear) bulk method requiring purification of cells that are sometimes rare in small samples of marrow or blood, immunoblots were used to confirm expression of lamins in a few cell-sample types. Quantitation of relative lamin levels by flow cytometry of a given lineage was done systematically using mean fluorescent intensity (MFI), and these measurements were then compared with lamin levels in a standard cell line (A549) for which the lamin-A:B ratio is calibrated by mass spectrometry (*SI Materials and Methods*).

**ACKNOWLEDGMENTS.** We thank Dr. Robert Goldman for lamin-B1 shRNA. This work was supported by National Institutes of Health Grants P01DK032094 and R01HL062352, and National Science Foundation and Human Frontier Science Program grants (to D.E.D.).

1. Sabin FR (1928) Bone marrow. *Physiol Rev* 8:151–190.
2. Lichtman MA (1970) Cellular deformability during maturation of the myeloblast: Possible role in marrow egress. *N Engl J Med* 283(18):943–948.
3. Lichtman MA, Packman CH, Constine LS (1989) Molecular and Cellular Traffic Across the Marrow Sinuses. *Handbook of the Hemopoietic Microenvironment*, ed Tavassoli M (Humana Press, Clifton, NJ).
4. Lam WA, Rosenbluth MJ, Fletcher DA (2007) Chemotherapy exposure increases leukemia cell stiffness. *Blood* 109(8):3505–3508.
5. Dechat T, Adam SA, Taimen P, Shimi T, Goldman RD (2010) Nuclear lamins. *Cold Spring Harb Perspect Biol* 2(11):a000547.
6. Pajerowski JD, Dahl KN, Zhong FL, Sammak PJ, Discher DE (2007) Physical plasticity of the nucleus in stem cell differentiation. *Proc Natl Acad Sci USA* 104(40):15619–15624.
7. Peric-Hupkes D, et al. (2010) Molecular maps of the reorganization of genome-nuclear lamina interactions during differentiation. *Mol Cell* 38(4):603–613.
8. Gerner C, Sauermann G (1999) Nuclear matrix proteins specific for subtypes of human hematopoietic cells. *J Cell Biochem* 72(4):470–482.
9. Röber RA, Sauter H, Weber K, Osborn M (1990) Cells of the cellular immune and hemopoietic system of the mouse lack lamins A/C: Distinction versus other somatic cells. *J Cell Sci* 95(Pt 4):587–598.
10. Olins AL, et al. (2008) The human granulocyte nucleus: Unusual nuclear envelope and heterochromatin composition. *Eur J Cell Biol* 87(5):279–290.
11. Guilly MN, Kolb JP, Gosti F, Godeau F, Courvalin JC (1990) Lamins A and C are not expressed at early stages of human lymphocyte differentiation. *Exp Cell Res* 189(1):145–147.
12. Dahl KN, et al. (2006) Distinct structural and mechanical properties of the nuclear lamina in Hutchinson-Gilford progeria syndrome. *Proc Natl Acad Sci USA* 103(27): 10271–10276.
13. Merideth MA, et al. (2008) Phenotype and course of Hutchinson-Gilford progeria syndrome. *N Engl J Med* 358(6):592–604.
14. Jahn D, et al. (2012) A truncated lamin A in the Lmna -/- mouse line: Implications for the understanding of laminopathies. *Nucleus* 3(5):463–474.
15. Hale JS, Frock RL, Mamman SA, Fink PJ, Kennedy BK (2010) Cell-extrinsic defective lymphocyte development in Lmna(-/-) mice. *PLoS ONE* 5(4):e10127.
16. Naetar N, et al. (2008) Loss of nucleoplasmic LAP2alpha-lamin A complexes causes erythroid and epidermal progenitor hyperproliferation. *Nat Cell Biol* 10(11):1341–1348.
17. Hoffmann K, et al. (2002) Mutations in the gene encoding the lamin B receptor produce an altered nuclear morphology in granulocytes (Pelger-Huët anomaly). *Nat Genet* 31(4):410–414.
18. Zwerger M, Herrmann H, Gaines P, Olins AL, Olins DE (2008) Granulocytic nuclear differentiation of lamin B receptor-deficient mouse EPRO cells. *Exp Hematol* 36(8): 977–987.
19. Okumura K, Nakamachi K, Hosoe Y, Nakajima N (2000) Identification of a novel retinoic acid-responsive element within the lamin A/C promoter. *Biochem Biophys Res Commun* 269(1):197–202.
20. Warrell RP, Jr., et al. (1991) Differentiation therapy of acute promyelocytic leukemia with tretinoin (all-trans-retinoic acid). *N Engl J Med* 324(20):1385–1393.
21. Andrade R, Alonso R, Peña R, Arlucea J, Aréchaga J (2003) Localization of importin alpha (Rch1) at the plasma membrane and subcellular redistribution during lymphocyte activation. *Chromosoma* 112(2):87–95.
22. Zermati Y, et al. (2001) Caspase activation is required for terminal erythroid differentiation. *J Exp Med* 193(2):247–254.
23. Krauss SW, et al. (2005) Nuclear substructure reorganization during late-stage erythropoiesis is selective and does not involve caspase cleavage of major nuclear substructural proteins. *Blood* 106(6):2200–2205.
24. Junt T, et al. (2007) Dynamic visualization of thrombopoiesis within bone marrow. *Science* 317(5845):1767–1770.
25. Oakes PW, et al. (2009) Neutrophil morphology and migration are affected by substrate elasticity. *Blood* 114(7):1387–1395.
26. Beadle C, et al. (2008) The role of myosin II in glioma invasion of the brain. *Mol Biol Cell* 19(8):3357–3368.
27. Scaffidi P, Misteli T (2008) Lamin A-dependent misregulation of adult stem cells associated with accelerated ageing. *Nat Cell Biol* 10(4):452–459.
28. Naito M, Omoteyama K, Mikami Y, Takagi M, Takahashi T (2012) Suppression of lamin A/C by short hairpin RNAs promotes adipocyte lineage commitment in mesenchymal progenitor cell line, ROB-C26. *Histochem Cell Biol* 137(2):235–247.
29. Kim Y, et al. (2011) Mouse B-type lamins are required for proper organogenesis but not by embryonic stem cells. *Science* 334(6063):1706–1710.
30. Labbaye C, et al. (1994) Retinoic acid downmodulates erythroid differentiation and GATA1 expression in purified adult-progenitor culture. *Blood* 83(3):651–656.
31. Purton LE, et al. (2006) RARgamma is critical for maintaining a balance between hematopoietic stem cell self-renewal and differentiation. *J Exp Med* 203(5):1283–1293.
32. Gronemeyer H, Gustafsson JA, Laudet V (2004) Principles for modulation of the nuclear receptor superfamily. *Nat Rev Drug Discov* 3(11):950–964.
33. Jung HJ, Lee JM, Yang SH, Young SG, Fong LG (2013) Nuclear lamins in the brain: New insights into function and regulation. *Mol Neurobiol* 47(1):290–301.
34. Swift J, et al. (2013) Nuclear lamin-A scales with tissue stiffness and enhances matrix-directed differentiation. *Science* 341(6149):1240104.
35. Vitrat N, et al. (1998) Endomitosis of human megakaryocytes are due to abortive mitosis. *Blood* 91(10):3711–3723.
36. Lammerding J, et al. (2006) Lamins A and C but not lamin B1 regulate nuclear mechanics. *J Biol Chem* 281(35):25768–25780.
37. Popova EY, et al. (2009) Chromatin condensation in terminally differentiating mouse erythroblasts does not involve special architectural proteins but depends on histone deacetylation. *Chromosome Res* 17(1):47–64.
38. Shimi T, et al. (2008) The A- and B-type nuclear lamin networks: Microdomains involved in chromatin organization and transcription. *Genes Dev* 22(24):3409–3421.
39. Hu J, et al. (2013) Isolation and functional characterization of human erythroblasts at distinct stages: Implications for understanding of normal and disordered erythropoiesis in vivo. *Blood* 121(16):3246–3253.

# Supporting Information

## Shin et al. 10.1073/pnas.1304996110

### SI Materials and Methods

**Cell Culture.** Fresh purified bone marrow-derived human $CD34^+$ cells and total mononuclear cells were obtained from either the Penn Xenograft Core Facility or AllCells (Emeryville, CA). Cells from at least five different donors were used in this study. Purity of the samples (>98%) was confirmed by flow cytometry with monoclonal antibody against human CD34. All experiments with primary cells were performed in primary hematopoietic media (StemLine-II; Sigma) supplemented with 1× antibiotics and the following human recombinant cytokines: stem cell factor (SCF; 100 ng/mL) and thrombopoietin (Tpo; 100 ng/mL). In some occasions, the media were also supplemented by fetal bovine serum (FBS) [10% (vol/vol)], dexamethasone (Sigma; 1 μM), 17β-estradiol (Sigma; 1 μM), granulocyte-colony stimulating factor (G-CSF; 10 ng/mL), erythropoietin (EPO; 1 U/mL), and interleukin-3 (IL-3, 1 ng/mL). All cytokines were purchased from R&D Systems. MEG01 and COS-1 cells were cultured in RPMI-1640 and DMEM, respectively, supplemented with 10% FBS and 1% antibiotics. In some cases, cells were treated with different doses of drugs after 7∼10 d of culture, including all-trans retinoic acid (RA) (Sigma), AGN 193109 (Santa Cruz Biotechnology), 17-(Allylamino)-17-demethoxygeldanamycin (17-AAG; Sigma), and anacardic acid (Sigma) for indicated durations of up to 3 d. Cells were cultured at 37 °C in 5% $CO_2$.

**Mass Spectrometry-Calibrated Intracellular Flow Cytometry.** Cells were fixed with 4% paraformaldehyde in PBS for 10 min, washed with PBS/1% BSA (staining medium), and incubated in 0.5% Triton X-100 for 10 min. After washing with the staining medium, samples were stained with antibodies against cytoplasmic antigens, including rabbit anti–lamin-A and goat anti–lamin-B (all from Santa Cruz Biotechnology) for 1 h at room temperature. In addition, cells were concurrently stained with Hoechst 33342 (Invitrogen) and lineage markers, including the following: phycoerythrin (PE) or APC (allophycocyanin)-Cy7 anti-CD34 (581; Invitrogen or Biolegend), PECy7 anti-CD38 (HIT2; eBioscience), PE anti-human CD33, PE anti-human CD19, PE anti-human CD3 (all from Biolegend), PE or APC anti-human glycophorin A (GPA) (Invitrogen), and FITC or APC anti-human CD41 (eBioscience). Cells were then washed and stained with anti-rabbit Alexa 488 and anti-goat Alexa 647 (Invitrogen) for 30 min, followed by analysis on LSR II flow cytometer (Becton Dickinson).

After intracellular flow cytometry to obtain the mean fluorescent intensity (MFI) values of lamin-A and lamin-B across different samples, each MFI value from flow cytometry was calibrated against mass spectrometry results with A549. From flow cytometry:

$$[A]_{\mathrm{A549}} \cdot \alpha = I^A_{\mathrm{A549}}$$
$$[B]_{\mathrm{A549}} \cdot \beta = I^B_{\mathrm{A549}},$$

where $[A]$ and $[B]$ represent concentrations of lamins A and B, $\alpha$ and $\beta$ are instrument response functions (in this case, direct proportionality), and $I$ is the mean fluorescence intensity in either lamin channel from flow cytometry. From mass spectrometry, the absolute ratio between isoforms is defined as $R$.

$$\frac{[A]_{\mathrm{A549}}}{[B]_{\mathrm{A549}}} = R_{\mathrm{A549}}$$

The estimate of $R_{A549}$ is 2.3. Combine instrument response functions into k, which can be defined from experimentally measureable terms (using A549 as a standard):

$$\frac{\alpha}{\beta} = \frac{I^A_{\mathrm{A549}}}{I^B_{\mathrm{A549}} \cdot R_{\mathrm{A549}}} = k,$$

k = 0.26. Other samples can then be characterized from flow cytometry measurements, based on calibration through this scaling factor:

$$\frac{[A]_x}{[B]_x} = \frac{I^A_x}{I^B_x \cdot k}$$
$$[A]_x + [B]_x = \frac{I^A_x}{\alpha} + \frac{I^B_x}{\beta} = \beta^{-1} \cdot \left(\frac{I^A_x}{k} + I^B_x\right)$$
$$[A]_x + [B]_x \propto \left(\frac{I^A_x}{k} + I^B_x\right).$$

**Western Blot Analysis.** Cells were washed with ice-cold PBS and lysed on ice with lysis buffer (150 mM sodium chloride, 1% Nonidet P-40, 1% protease inhibitor mixture 50 mM Tris at pH 8.0) mixed with 1× NUPAGE LDS sample buffer (Invitrogen) for 30 min with sonication. Samples were then boiled for 10 min at 90∼100 °C, followed by centrifugation for 5 min at 11,200 × $g$. For Western blot, whole lysates were separated on 3–7% NUPAGE Tris-Acetate gels (Invitrogen). The proteins were then transferred to a polyvinylidene fluoride (PVDF) membrane with an iBlot Gel Transfer Device (Invitrogen), followed by blocking with 5% nonfat dry milk solution for 1 h. Incubation with primary antibodies was done at 4 °C overnight with 1:1,000 total rabbit anti–lamin-A or goat anti–lamin-B (Santa Cruz Technology). After washing, the membrane was incubated with 1:2,500 anti-rabbit and 1:1,000 anti-goat HRP-conjugated IgG antibodies at room temperature for 1 h. The blot was developed with ChromoSensor (GenScript) for 5 min, followed by digital scanning to perform densitometry analysis by ImageJ (National Institutes of Health).

**Micropipette Analysis.** Primary cells or cell lines in suspension were subjected to micropipette analysis. Capillary tubes of 1.0 mm inner diameter (World Precision Instruments) were pulled into micropipettes using a Flaming-Brown Micropipette Puller (Sutter Instrument) and cut further using a deFonbrune-type microforge (Vibratome). The average micropipette diameter was around 3 μm. Micropipettes were attached to a dual-stage water manometer with reservoirs of adjustable height. Suction was applied by a syringe, and the corresponding pressure was measured by pressure transducer (Validyne) calibrated by a mercury U-tube manometer. Pressures for different experiments ranged from 0.5 to 15 kPa.

**Pore-Migration Assay.** Migration of hematopoietic cells was measured in a modified Boyden chamber migration assay using Transwell inserts with a 3-, 5-, and 8-μm porous membrane (Millipore). Cells were loaded into the migration chamber in a serum-free condition. Medium containing 100 ng/mL stromal derived factor-1 (SDF-1) (Peprotech) was placed in the lower chamber in some studies. After allowing cell migration for 4 h, cells were removed from the lower chamber as well as the upper side of membranes. The number and type of migratory cells were evaluated by flow cytometry with defined number of fluorescent beads (APC conjugated, Becton Dickinson) and staining cells with lineage markers as used in mass spectrometry-calibrated intracellular flow (MS-IF) cytometry. To evaluate the effect of drugs or RNAi of lamins on migration, cells were pretreated with RA, lamin-A

siRNA, or lamin-B shRNA for 3 d before loading onto the migration chamber.

**Introduction of Nucleic Acids in Vitro.** $CD34^+$-derived cells or MEG01 cells were transfected with GFP-lamin-A (wild-type or mutants) or lamin-A siRNA by electroporation ("nucleofection") using the Nucleofector kits (Lonza) as described in the manual. Briefly, cultured cells were washed with PBS and resuspended with transfection solution containing 2 μg/mL DNA constructs or 3 μg/mL siRNA. They were then transferred into a cuvette and transfected with the Nucleofector II. The medium at 37 °C was then added to transfected cells. Cells were incubated overnight, and then the medium was exchanged to fresh on the next day.

To silence the expression of lamin-B1, the retrovirus vector constructs containing shRNA were obtained from the laboratory of Robert Goldman (Northwestern University, Chicago) and prepared as described previously (1). pSilencer constructs containing either scrambled or lamin-B1 shRNA sequences were transfected into HEK-293T cells, and virus-containing culture supernatants were collected at 24~48 h following transfection in serum-free hematopoietic media. The culture supernatants containing virus were then incubated with $CD34^+$-derived cells for shRNA transduction in the presence of 5 μg/mL polybrene (Sigma) and incubated for 1 d. Virally transduced cells were selected by adding 1 μg/mL puromycin (Invitrogen) for 2 d and incubated in fresh medium for at least 1 d before further analyses. Lamin-A was also down-regulated stably in a similar manner as lamin-B1 with human lamin-A shRNA (Sigma).

For lamin-A promoter assays, we used a GFP construct driven by the human lamin-A promoter cloned by Genecopoeia. The promoter was derived from the 1,132-base pair upstream region and the first 385-base pair mRNA transcript region. Promoter activity was characterized with or without retinoic acid after transient transfection using LF2k (Invitrogen) per the manufacturer's instructions.

**Colony-Forming Assay.** One thousand to 3,000 $CD34^+$-derived cells were seeded into methylcellulose-containing media (MethoCult H4434; StemCell Technologies) supplemented with SCF, GM-CSF, IL-3, and Epo. They were cultured for 14 d, and colonies were scored at 10× magnification based on the published morphological criteria by StemCell Technoloigies. Colony-forming content was normalized per 10,000 cells seeded.

**Image Acquisition and Analysis.** Cells on coverslips were fixed with 4% paraformaldehyde, followed by permeabilization with 0.5% Triton X-100 in PBS for 15 min and blocking with 1% BSA in PBS for 30 min. Samples were then stained with primary antibodies (1:100 for all antibodies used) for overnight at 4 °C. After washing, staining with appropriate Alexa 488 or 647-conjugated secondary antibodies (1:400) and TRITC-phalloidin was performed for 45 min at room temperature. Cells were washed three times with PBS and mounted in ProLong Gold antifade medium (Invitrogen). Samples were then analyzed by fluorescence or confocal microscopy.

**Live Cell Imaging Analysis.** Cells transfected with GFP-lamin-A were put into Ibidi μ-slide VI (Ibidi GmbH) in cell-culture medium. Analysis was done in an insulated chamber maintained at 37 °C, 5% $CO_2$. A series of images were collected every 5 min for ~18 h with an Olympus IX70 inverted microscope with 300W Xenon lamp illumination using 20× objectives under bright field and fluorescence. Image stacks were further analyzed by ImageJ to analyze lamin-A distribution during polyploidization.

**Mass Spectrometry Analysis of Posttranslational Modification.** Sample preparation and subsequent analysis by mass spectrometry were performed in duplicate. Gel electrophoresis was performed as described previously. Gel sections were washed [50% 0.2 M ammonium bicarbonate (AB) solution, 50% acetonitrile (ACN), 30 min at 37 °C], dried by lyophilization, incubated with a reducing agent [20 mM Tris(2-carboxyethyl)phosphine (TCEP) in 25 mM AB solution at pH 8.0, 15 min at 37 °C], and alkylated [40 mM iodoacetamide (IAM) in 25 mM AB solution at pH 8.0, 30 min at 37 °C]. The gel sections were dried by lyophilization before in-gel trypsinization [20 μg/mL sequencing grade modified trypsin in buffer as described in the manufacturer's protocol (Promega), 18 h at 37 °C with gentle shaking]. The resulting solutions of tryptic peptides were acidified by addition of 50% digest dilution buffer (60 mM AM solution with 3% methanoic acid).

Peptide separations (5 μL injection volume) were performed on 25-cm PicoFrit column (75-μm inner diameter; New Objective) packed with Magic 3 μm C18 reversed-phase resin (Michrom Bioresources) using a nanoflow HPLCy system (Eksigent Technologies), which was coupled online to a hybrid LTQ-Orbitrap XL mass spectrometer (Thermo Fisher Scientific) via a nanoelectrospray ion source. Chromatography was performed with Solvent A (Milli-Q water with 0.1% formic acid) and Solvent B (acetonitrile with 0.1% formic acid). Peptides were eluted at 200 nL/min for 3–28% B over 42 min, 28–50% B over 26 min, 50–80% B over 5 min, 80% B for 4.5 min before returning to 3% B over 0.5 min. To minimize sample carryover, a fast blank gradient was run between each sample. The LTQ-Orbitrap XL was operated in the data-dependent mode to automatically switch between full scan MS ($m/z$ = 300–2,000 in the orbitrap analyzer (with resolution of 60,000 at $m/z$ 400) and the fragmentation of the six most intense ions by collision-induced dissociation in the ion trap mass analyzer.

Raw mass spectroscopy data were processed using Elucidator (version 3.3; Rosetta Biosoftware). The software was set up to align peaks in data from samples derived from corresponding molecular weight regions of the 1D gels. Peptide and protein annotations were made using SEQUEST (version 28; Thermo Fisher Scientific) with full tryptic digestion and up to two missed cleavage sites. Peptide masses were selected between 800 and 4,500 amu with peptide mass tolerance of 1.1 amu and fragment ion mass tolerance of 1.0 amu. Peptides were searched against databases compiled from UniRef100 (November 2010 database) human plus contaminants and a reverse decoy database. Only proteins detected with three or more peptides were considered for quantification. The peptide database was modified to search for alkylated cysteine residues (monoisotopic mass change, $\Delta$ = +57.021 Da), oxidized methionine ($\Delta$ = +15.995 Da), acetylated lysine ($\Delta$ = +42.011 Da), methylated lysine and arginine ($\Delta$ = +14.016 Da), and phosphorylated serine, tyrosine, threonine, histidine, and aspartate ($\Delta$ = +79.966 Da). The absolute ratio between protein isoforms (lamin A:B) was determined by consideration of peptides common to both forms, as described elsewhere (2). The relative signals of posttranslationally modified peptides were quantified as fractions of the average ion current of other peptides from the same parent protein.

**Statistical Analyses.** All statistical analyses were performed using GraphPad Prism 5. Unless noted, all statistical comparisons were made by unpaired 2-tailed Student $t$ test and were considered significant if $P < 0.05$. Dose–response data were fit to sigmoidal dose–response of variable slope with $x$ axis in a log scale.

## Supplemental Discussion of Cortical Rigidity Versus Lamina Rigidity

The lamin expression pattern in our study is further supported by measurement of nuclear rheology. Very few studies have directly measured the mechanical properties of leukocyte nuclei. For lymphoid, one study suggests a nuclear cortical tension in T cells of ~2 mN/m (3), which is only twofold larger than the cortical tension required to fragment megakaryocytes (MKs) (2), consistent with the notion that lymphocytes down-regulate both lamin isoforms (Fig. 1*F*) and are highly deformable through pores (Fig. 2 and Fig. S3*B*). No cell intrinsic effect was observed in lymphocytes from lamin-A/C perturbed mice (4), consistent with low lamin levels.

Programming of cellular deformability during granulopoiesis has been suggested by micropipette (5) and microfluidic optical stretcher (6) methods, but these studies do not distinguish the contribution of cell cortex from that of the nucleus. Cortical stiffness is regulated by actomyosin forces via nonmuscle myosin-II (NMM-II) (7), and so we measure nuclear deformability in situ with latrunculin-A treatment to inhibit actomyosin forces (8). As demonstrated in the MK lineage, the expression of NMM-II is also dynamically regulated during terminal differentiation (2), which suggests that cortical deformability is also dynamically programmed in hematopoiesis. An obvious distinction here is that, whereas actin-myosin can generate force and contribute to "active" migration via adhesion and crawling, lamins are intermediate filaments that do not generate force, but their contributions to rigidity can limit migration. Relationships between nuclear and cortical elasticity in hematopoiesis need further study.


1. Shimi T, et al. (2011) The role of nuclear lamin B1 in cell proliferation and senescence. *Genes Dev* 25(24):2579–2593.
2. Shin JW, Swift J, Spinler KR, Discher DE (2011) Myosin-II inhibition and soft 2D matrix maximize multinucleation and cellular projections typical of platelet-producing megakaryocytes. *Proc Natl Acad Sci USA* 108(28):11458–11463.
3. Dong C, Skalak R, Sung KL (1991) Cytoplasmic rheology of passive neutrophils. *Biorheology* 28(6):557–567.
4. Hale JS, Frock RL, Mamman SA, Fink PJ, Kennedy BK (2010) Cell-extrinsic defective lymphocyte development in Lmna(-/-) mice. *PLoS ONE* 5(4):e10127.
5. Lichtman MA (1970) Cellular deformability during maturation of the myeloblast: Possible role in marrow egress. *N Engl J Med* 283(18):943–948.
6. Lautenschläger F, et al. (2009) The regulatory role of cell mechanics for migration of differentiating myeloid cells. *Proc Natl Acad Sci USA* 106(37):15696–15701.
7. Merkel R, et al. (2000) A micromechanic study of cell polarity and plasma membrane cell body coupling in Dictyostelium. *Biophys J* 79(2):707–719.
8. Pajerowski JD, Dahl KN, Zhong FL, Sammak PJ, Discher DE (2007) Physical plasticity of the nucleus in stem cell differentiation. *Proc Natl Acad Sci USA* 104(40):15619–15624.


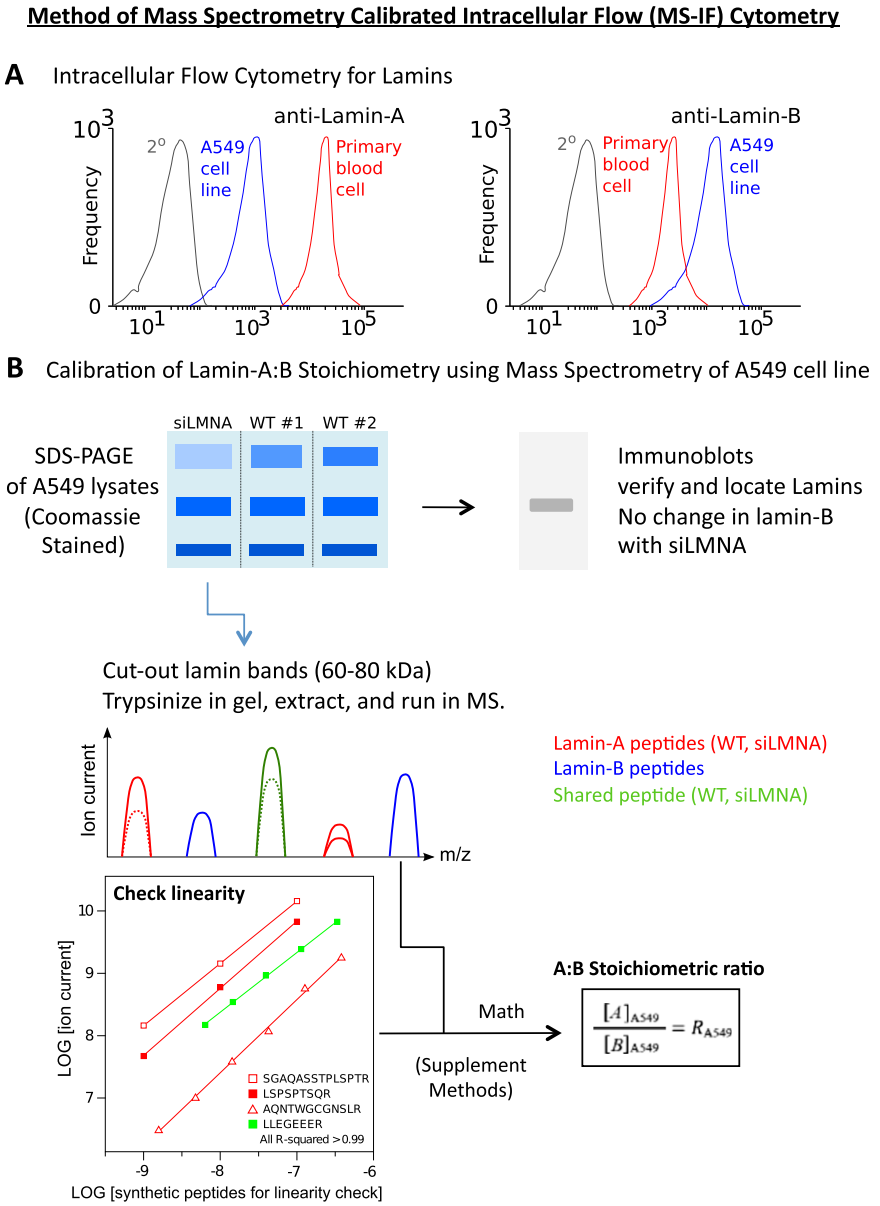


**Fig. S1.** Schematics of MS-IF-cytometry. (*A*) Representative plots showing lamin isoform expressions measured by intracellular flow cytometry. (*B*) Determination of absolute lamin-A:B ratios by calibrating flow cytometry results with mass spectometry. A549 was used as a standard. Detailed description is available in *SI Materials and Methods*.

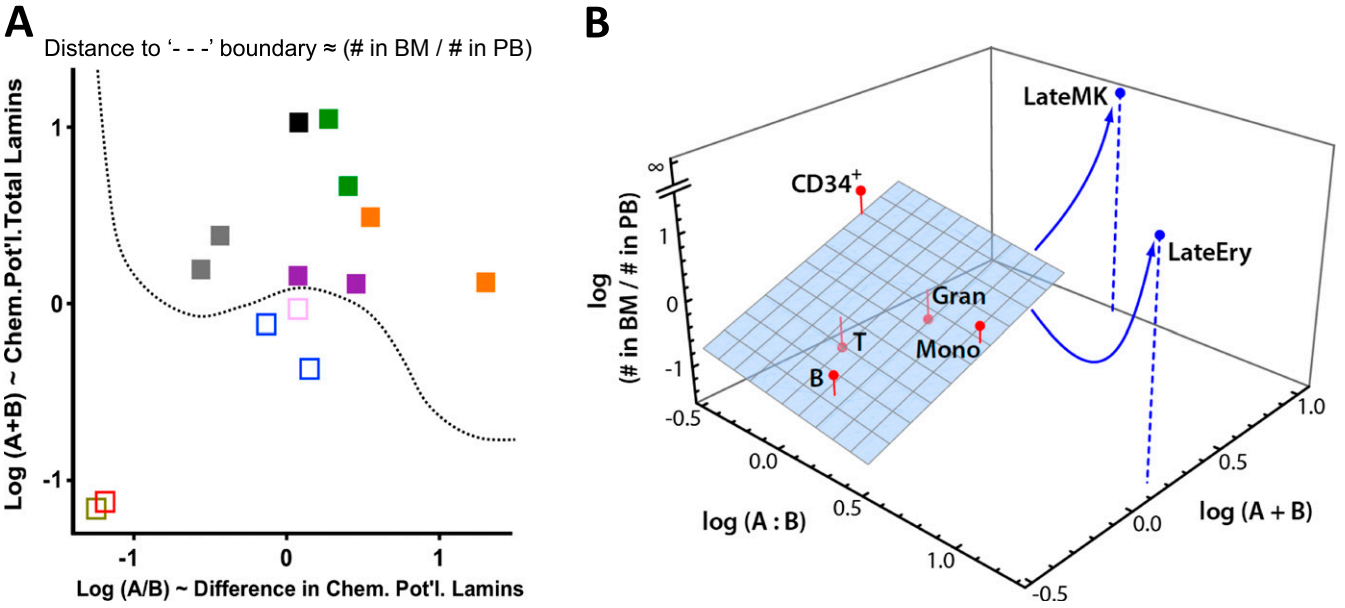


**Fig. S2.** Lamins and hematopoietic lineage distribution in marrow and blood. (*A*) Distribution of hematopoietic lineages expressed using the standard definition of chemical potential (Chem. Pot'l) as the logarithm of a relative concentration in a cell or nucleus. Distances from the curvilinear barrier to each point reflect known distribution of lineages between marrow and peripheral blood. (*B*) Log plot showing the relationship between lamin isoform ratio, total lamin intensity, and bone marrow (BM) to peripheral blood (PB) cell ratio. To formally assess the dependence of marrow/blood partitioning on the two coordinates of the lamin lineage map, literature values for known marrow-to-blood distributions were fitted for $CD34^+$, myeloid, and lymphoid lineages. Data from fresh $CD34^+$, T, B, granulocyte (Gran), and monocyte (Mono) were fit to a surface defined by the equation $z = A\,(x - b) + C\,(y - d)$ ($R^2 = 0.61$). Late MK and Late Ery are known to have very high BM:PB cell ratios and are not considered in the fit. Small deviations from a simple linear fit of the log data indicate that lamins contribute to compartmentalization of blood lineages.

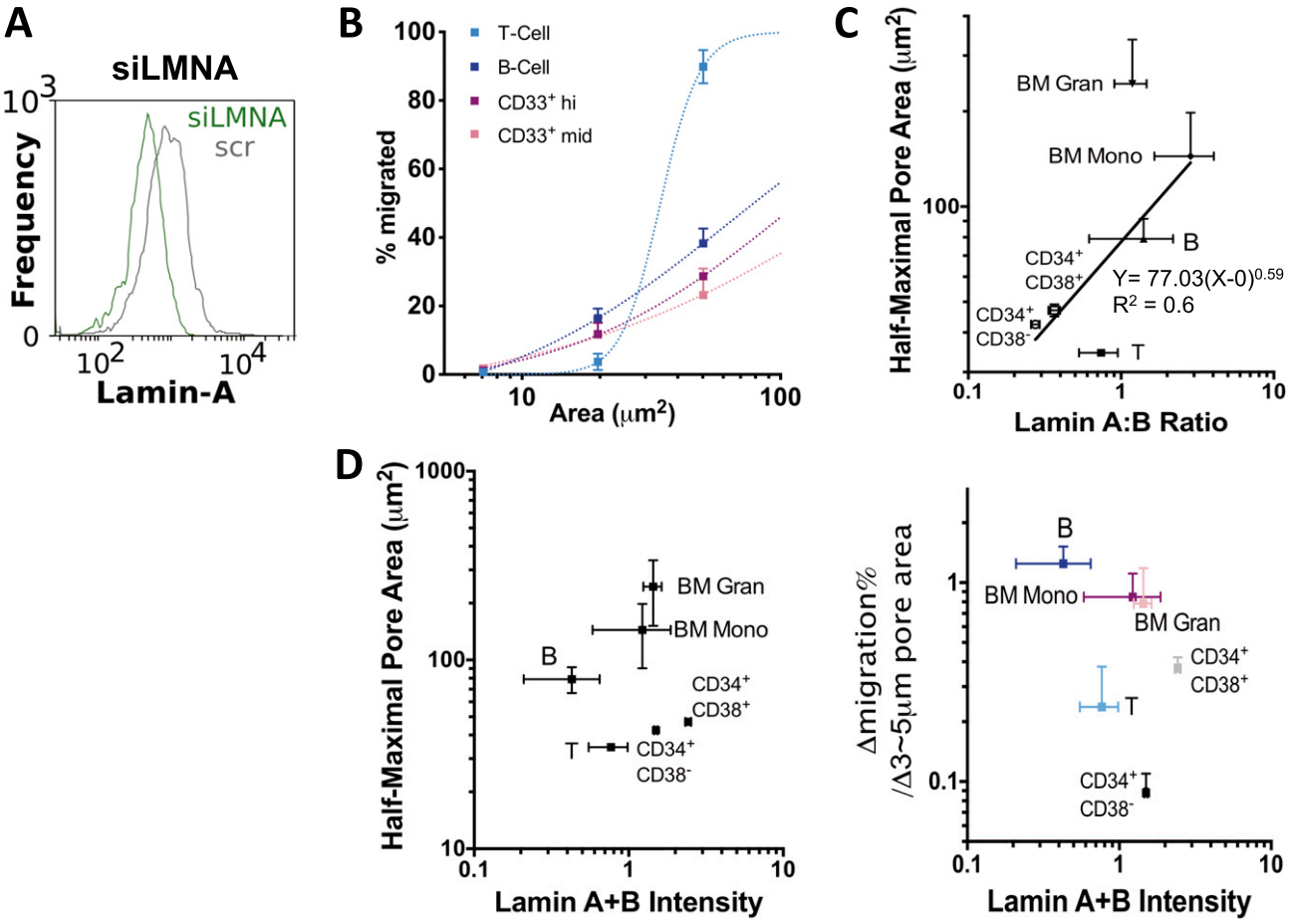


**Fig. S3.** 3D migration of hematopoietic lineages. (*A*) siRNA knockdown down-regulates lamin-A uniformly. Representative flow cytometry plot is shown. (*B*) Data from migration assays were fitted as in Fig. 2*B*, where A = 100 and (B, Xc, m): (T cell: 0.03, 1.44, 5.51), (B cell: 0.01, 6.64, 0.95), (CD33$^+$ hi, monocyte: 0.009, 5.00, 1.00), (CD33$^+$ mid, granulocyte, 0.005, 5.00, 0.79). (*C*) Correlation analysis between half-maximal pore area ($\mu m^2$) of migration ($A_{1/2}$) and lamin A:B ratios, where $A_{1/2} = Xc + 1/B$. See also Fig. 2*B*. The data were fitted with a power law, $Y = 77.03X^{0.59}$, $R^2 = 0.6$ for all data. (*D*, *Left*) Correlation analysis between $A_{1/2}$ and lamin total intensity. (*Right*) Correlation analysis between migration sensitivity, Y = Δ (% Migrated)/Δ (Pore Area) between 3- and 5-μm pores, and lamin total intensity. For all graphs, mean ± SEM of $n = 3$.

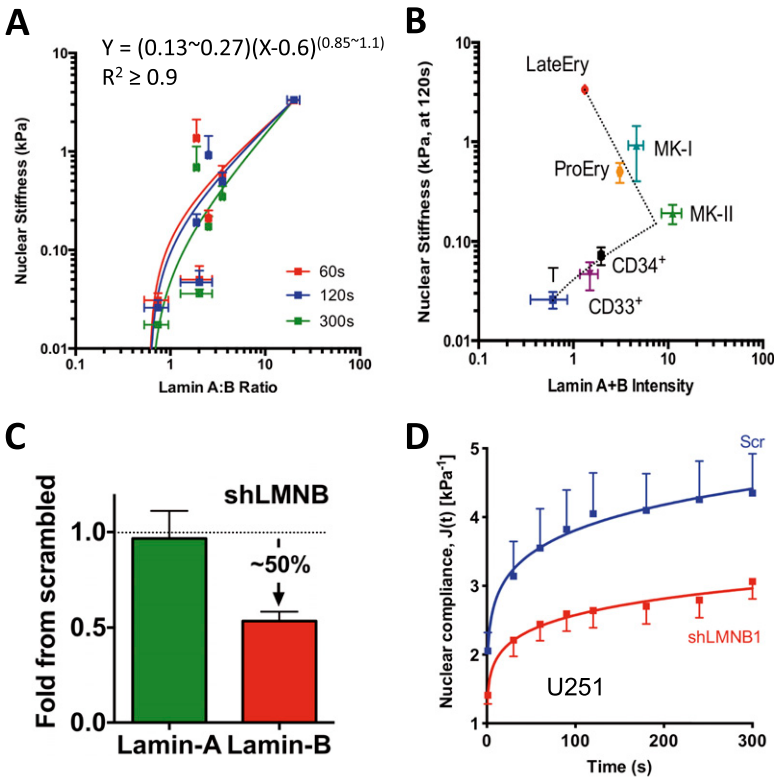


**Fig. S4.** Correlation analysis between nuclear stiffness and lamins. (*A*) Correlation between nuclear stiffness and lamin A:B ratio at 60, 120, and 300 s after aspiration under constant pressure. The graph was fitted with a power law, $Y = (0.13\sim0.27)(X\text{-}0.6)^{(0.85\sim1.1)}$, $R^2 \geq 0.9$. Mean ± SEM of $n \geq 5$ for each cell type. (*B*) Correlation analysis between nuclear stiffness and lamin total intensity at 120 s after aspiration. The graph was fitted with a power law, $Y = 0.05(X\text{-}0.32)^{0.55}$, $R^2 \geq 0.8$ for T cell, $CD33^+$, $CD34^+$, and MK-II, whereas $Y = 5.50X^{-1.80}$, $R^2 \geq 0.9$ for LateEry, ProEry, MK-I and MK-II. (*C*) Lamin-B shRNA down-regulates lamin-B without affecting lamin-A ($n = 3$ donors, $P < 0.05$). (*D*) Nuclear stiffening of U251 cells after lamin B1 knockdown. Nuclear compliance change with time under constant pressure $\Delta P \leq 3$ kPa over time with a power law fit, $J(t)$ ($kPa^{-1}$) = $A \cdot t^B$ (t = sec), where (A, B):): (scrambled (scr): 2.05, 0.13), (shLMNB1: 1.43, 0.13), $n = 5$, $P < 0.05$, scrambled vs. shLMNB1 at each time point, paired *t* test.

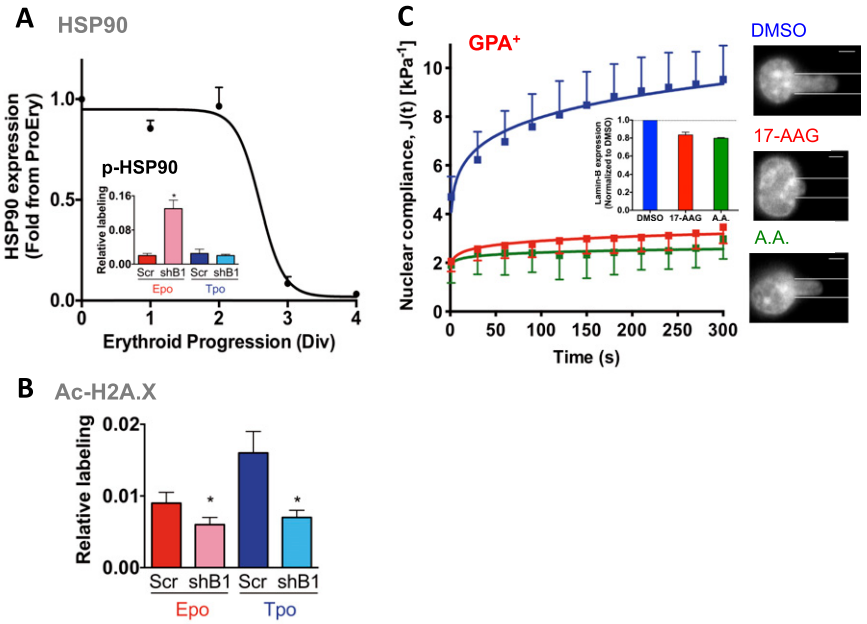


**Fig. S5.** Perturbation of physiological pathways can phenocopy the stiffening of nuclei with lamin-B down-regulation. Many other proteins change during erythropoiesis, and we hypothesized that, if we pharmacologically perturbed important erythropoietic pathways, then we should be able to phenocopy lamin-B changes as intrinsic to a common erythropoietic program. To first identify candidate targets, we performed quantitative mass spectrometry analyses of erythroid cells both without and with lamin-B1 RNAi treatment, which promotes BFU-Es. (*A*) HSP90 protein down-regulated during late erythropoiesis based on mass spectometry profiling of erythropoietic cells at five distinct stages of differentiation (1), consistent with a role for HSP90 in hematopoietic differentiation (2). (*Inset*) HSP90 phosphorylation levels at Ser226 and Ser255 (involved in drug resistance of cancer cells) (3) are up-regulated by lamin-B1 knockdown only in the presence of Epo. (*B*) Histone acetylation of H2A.X at Lys120 is decreased by lamin-B1 knockdown. (*C*) HSP90 and histone acetyltransferase inhibitors stiffen nuclei in erythropoiesis. $GPA^{+}$ erythroblasts were treated with the HSP90 inhibitor 17-AAG (60 nM) or with the histone acetyltransferase inhibitor anacardic acid (A.A., 20 μM) for 1 d, followed by micropipette aspiration of nuclei. Although $GPA^{+/hi}$ cells generally have stiffer nuclei than $GPA^{lo}$ (ProEry), all nuclei largely flow irreversibly at constant pressure. Both drugs phenocopy the stiffening of erythroblast and the decrease in lamin-B. Nuclear compliance change with the power law fit (*a, b*): (DMSO: 4.1, 0.14), (17-AAG 60 nM: 1.9, 0.09), [Anacardic Acid (A.A.) 10 μM: 1.9, 0.05] $P < 0.05$ ($n = 5$), DMSO vs. 17-AAG or A.A. for each time point in paired *t* test. (*Inset*) Graph shows down-regulation of lamin-B with both 17-AAG and A.A. One-way ANOVA $*P < 0.05$, Mean ± SD. (Scale bars: 3 μm.)


1. Hu J, et al. (2013) Isolation and functional characterization of human erythroblasts at distinct stages: Implications for understanding of normal and disordered erythropoiesis in vivo. *Blood* 121(16):3246–3253.
2. Grebenová D, et al. (2006) The proteomic study of sodium butyrate antiproliferative/cytodifferentiation effects on K562 cells. *Blood Cells Mol Dis* 37(3):210–217.
3. Kurokawa M, Zhao C, Reya T, Kornbluth S (2008) Inhibition of apoptosome formation by suppression of Hsp90beta phosphorylation in tyrosine kinase-induced leukemias. *Mol Cell Biol* 28(17):5494–5506.

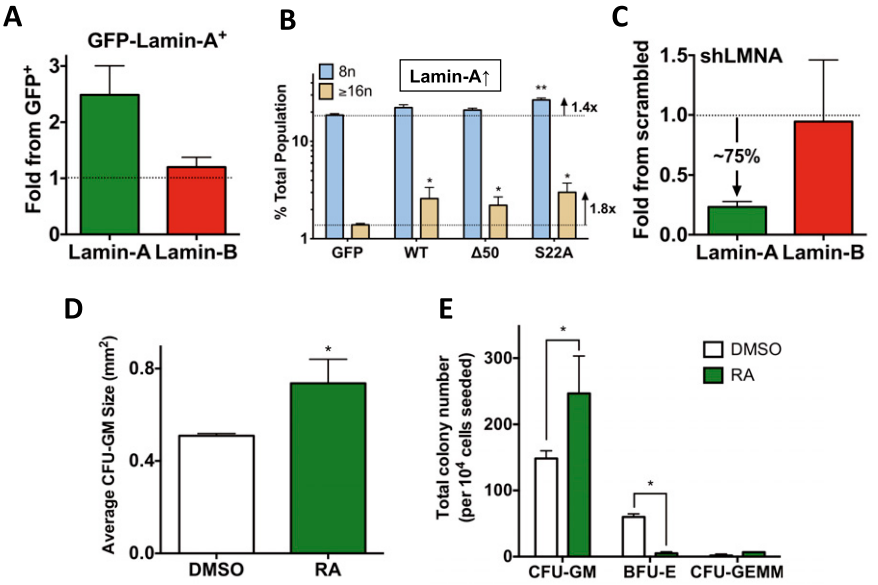


**Fig. S6.** (*A*) GFP–lamin-A overexpression increases lamin-A by 2.5-fold compared with GFP control ($n = 3$ donors, $P < 0.05$, mean ± SEM). (*B*) Lamin-A enhances MK polyploidization. Overexpression of GFP, wild-type (WT), Progerin mutant (Δ50), and phospho-deficient (S22A) mutant of lamin-A in MEG01 cells. $^{**}P < 0.05$, GFP vs. S22A 8n. $^{*}P < 0.05$, GFP vs. WT, Δ50 or S22A ($n = 4$). (*C*) Lamin-A shRNA down-regulates lamin-A selectively by 75% whereas lamin-B remains unchanged ($n = 3$ donors, $P < 0.05$, mean ± SEM). (*D*) Retinoic acid increases the mean size of CFU-GM. (*E*) Retinoic acid increases the number of CFU-GM whereas it decreases that of BFU-E ($n = 2$ donors, $P < 0.05$, mean ± SEM).

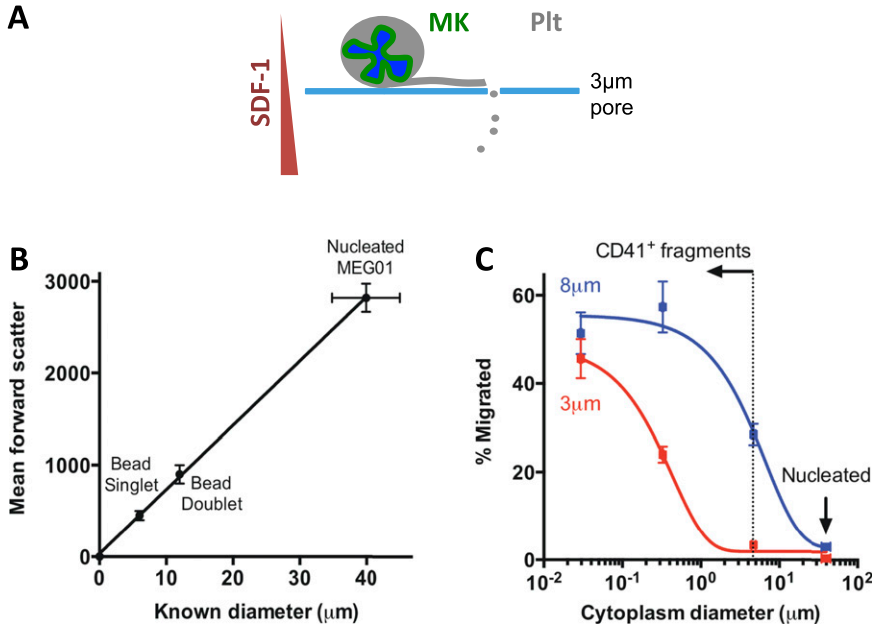


**Fig. S7.** Migration of nucleated MKs and platelet fragments through pores. (*A*) Illustration of nucleated MKs and platelets (plt) migrating through 3-μm pores under SDF-1 gradient. (*B*) Size calibration between forward scatter values from flow cytometry and known diameter of beads and MEG01 cells (measured by light microscopy), assuming that each cell or fragment is circular. Mean ± SEM, $n = 3$. (*C*) Migration of $CD41^{+}7\text{-}AAD^{-}$ fragments and nucleated cells from MEG01 through 3- and 8-μm pores. Cytoplasm diameter was extrapolated as in *B* assuming that each fragment or nucleated cell is circular. Exponential decay fit, half-life: 3-μm pore = 0.3 μm, 8-μm pore = 4.6 μm. $R^2 > 0.98$, mean ± SEM, $n = 3$.

**Table S1. Lamin-A and lamin-B expression values calibrated by MS-IF**

| Cell type | Lamin-A | Lamin-B | A:B | A+B | A:C (WB) |
|---|---|---|---|---|---|
| A549 | 2.30 | 1.00 | 2.3* | 3.30 | 0.78 ± 0.06 |
| MSC | 4.95 | 4.10 | 1.20 | 9.05 | 1.1 |
| $CD34^+CD38^-$ | 0.27 ± 0.02 | 1.00 ± 0.03 | 0.28 | 1.27 | 1.6 |
| $CD34^+CD38^+$ | 0.55 ± 0.06 | 1.51 ± 0.03 | 0.37 | 2.06 | |
| ProEry | 2.05 ± 0.10 | 0.58 ± 0.01 | 3.54 | 2.63 | 0.17 |
| LateEry | 1.07 ± 0.00 | 0.05 ± 0.01 | 19.66 | 1.12 | 0.95 |
| MKP | 2.75 ± 0.41 | 1.20 ± 0.17 | 2.28 | 3.95 | N/A |
| MK | 6.09 ± 0.79 | 3.39 ± 0.53 | 1.79 | 9.48 | N/A |
| BM M | 0.58 ± 0.25 | 0.24 ± 0.04 | 2.44 | 0.82 | N/A |
| BM G | 0.64 ± 0.03 | 0.58 ± 0.18 | 1.09 | 1.22 | N/A |
| B Cell | 0.18 ± 0.11 | 0.19 ± 0.08 | 0.96 | 0.37 | N/A |
| T Cell | 0.27 ± 0.11 | 0.38 ± 0.11 | 0.71 | 0.65 | N/A |
| PB G/M | 0.34 ± 0.13 | 0.54 ± 0.17 | 0.62 | 0.88 | N/A |

*Mass spectrometry measurement.

**Table S2. Percentage of nucleated hematopoietic lineages in marrow and blood**

| | % of leukocytes | | |
|---|---|---|---|
| Cell type | Marrow | Blood | Refs. |
| T cell | 9.8 | 25 | 1, 2 |
| B cell | 3.3 | 4 | 1, 2 |
| $CD33^{mid}$ (gran) | 50.0 | 70 | 1, 2 |
| $CD33^{hi}$ (mono) | 10.0 | 5 | 1, 2 |
| Nucleated erythroid | 28.5 | Very low | 1, 2 |
| Nucleated MK | 1.3 | Very low | 2 |
| $CD34^+$ | 0.8 | 0.06 | 3,4 |


1. Fauci AS, et al., eds (2009) *Harrison's Manual of Medicine* (McGraw-Hill, New York), 17th Ed.
2. Lee GR, et al., eds (1999) *Wintrobe's Clinical Hematology* (Lippincott Williams & Wilkins, Baltimore), 10th Ed.
3. McKenna DH, Jr, et al. (2010) CD34(+) cell selection using small-volume marrow aspirates: A platform for novel cell therapies and regenerative medicine. *Cytotherapy* 12(2):170–177.
4. Anonymous (2012) *Frequencies of Cell Types in Human Peripheral Blood* (StemCell Technologies, Vancouver, BC, Canada).


**Table S3. Concentration of total nucleated hematopoietic cells in marrow and blood**

| Measurement | Marrow | Blood | Marrow/blood | Refs. |
|---|---|---|---|---|
| Nucleated cells/mL, $\times 10^7$ | 2.5 | 0.75 | 3.33 | 1, 2 |
| Total volume, mL | 541 | 5,000 | 0.11 | 3 |


1. McKenna DH, Jr., et al. (2010) CD34(+) cell selection using small-volume marrow aspirates: A platform for novel cell therapies and regenerative medicine. *Cytotherapy* 12(2):170–177.
2. Hoffman R, et al., eds (2008) *Hematology: Basic Principles and Practice* (Elsevier, Philadelphia), 5th Ed.
3. Sambuceti G, et al. (2012) Estimating the whole bone-marrow asset in humans by a computational approach to integrated PET/CT imaging. *Eur J Nucl Med Mol Imaging* 39(8): 1326–1338.

**Table S4. Total estimated number of nucleated hematopoietic lineages in marrow and blood**

| Cell type | Cell no., $\times 10^7$ | | |
|---|---|---|---|
| | Marrow | Blood | Marrow/blood |
| Total nucleated | 1,353 | 3,750 | 0.36 |
| T cell | 133 | 938 | 0.14 |
| B cell | 44 | 150 | 0.30 |
| $CD33^{mid}$ (gran) | 676 | 2,625 | 0.26 |
| $CD33^{hi}$ (mono) | 135 | 188 | 0.72 |
| Nucleated erythroid | 385 | Close to 0 | Close to ∞ |
| Nucleated MK | 17 | Close to 0 | Close to ∞ |
| $CD34^+$ | 10 | 2 | 4.63 |

**Table S5. Mass spectometry measurement of lamin B1 and B2 expression levels in a range of hematopoietic and cultured cell lines**

| Cell type | Lamin B1:B2 (median ion current) | Lamin B1: B2 (peptide count) | LMNB1 Wb | LMNB2 Wb |
|---|---|---|---|---|
| $CD34^+$ | 4: 1 | 18: 9 | ◎ | ◎ |
| EPO | 6: 1 | ND | ND | ND |
| Pro | 20: 1* | 19: 0 | ND | ND |
| E Baso | 30: 1* | 21: 0 | ND | ND |
| L Baso | 35: 1* | 24: 0 | ND | ND |
| Poly | 3: 1 | 24: 12 | ND | ND |
| Ortho | 4: 1 | 17: 5 | ND | ND |
| TPO | 8: 1 | ND | ND | ND |
| MEG01 | 3: 1 | 14: 1 | ◎ | C |
| MKP | Lamin B2 not detected | 6: 0 | ND | ND |
| MK | Lamin B2 not detected | 6: 0 | ND | ND |
| MSC | 0.7: 1 | 4: 6 | ◎ | C |
| U251 | 1.6: 1 | 19: 12 | ● | ◎ |
| A549 | 1.8: 1 | 17: 10 | ● | ◎ |

Proteins detected in mass spectometry experiments were quantified in two ways: by counting the number of tryptic peptides uniquely derived from each lamin isoform ("peptide count") and by comparing the median signal strength of those peptides ("median ion current"). Both methods give approximate and generally comparable measures of relative protein concentration, and as lamin-B1 and -B2 are of similar size and detectability, ratios of these values give an estimate of the lamin-B1: B2 composition. In samples where low levels of lamin-B2 became difficult to detect, the MS spectra were aligned with those from an A549 standard sample to record the ion currents. Where sufficient cell lysate was available, MS measurements were validated by qualitative WB using antibodies specific to lamin-B1 or B2. Although both B-type lamins show similar detectability in cultured cell lines, lamin-B1 becomes dominant during hematopoietic differentiation. ND, not determined; ○, no band; ◎, weak; ●, strong. EPO, Epo-cultured $CD34^+$-derived cells; Pro, proerythroblast; E Baso, early basophilic erythroblast; L Baso, late basophilic erythroblast; Poly, polychromatic erythroblast; Ortho, orthochromatic erythroblast; TPO, Tpo-cultured $CD34^+$-derived cells; MKP, megakaryocyte progenitors; MK, megakaryocytes; MSC, mesenchymal stem cells.
*Lamin B2 only detected with alignment.

**Table S6. Representative images showing results from Western blot validation of lamin B1 and B2 expression levels**

| | MSC | U251 | A549 | MEG01 | CD34$^+$ |
|---|---|---|---|---|---|
| LMNB1 |  | 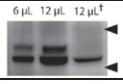 |  |  | 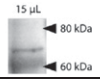 |
| LMNB2 |  | 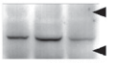 |  |  |  |